CHAPTER FIVE

PERFORMANCE EVALUATION PLATFORMS

5.1 CHAPTER OVERVIEW

THE first part of this chapter details the operation of the general baseband complex QPSK transmitter and receiver structures [81] employed in the AWGN and flat fading channel simulations of *Chapter* 6. Also briefly described is the estimation of the average fading amplitude associated with each of the individual demodulated QPSK receiver output data bit estimates. Analytical BER performances for uncoded coherently demodulated QPSK communication systems, functioning in a variety of mobile radio channel conditions, is the final topic discussed in this part of the chapter.

The baseband complex DS/SSMA QPSK transmitter and RAKE receiver structures [47] employed in the frequency selective fading channel simulations of *Chapter* 6 are the first topics discussed in the second part of this chapter. This is followed by a discussion on the estimation of the average fading amplitude associated with each of the RAKE receiver output data bit estimates. A concise derivation of an approximate BER curve for the wideband transmitter and RAKE receiver structures concludes this part of the chapter.

Considered in the third and final part of this chapter is the general simulation platforms employed in *Chapter* 6. This includes the transmitter and receiver setups for both the narrowband QPSK and wideband DS/SSMA QPSK communication systems employed, as well as a comprehensive overview of the wide variety of AWGN, flat fading and multipath fading channel configurations considered.

5.2 NARROWBAND COMPLEX QPSK COMMUNICATION SYSTEMS

The following subsections describe the general transmitter and receiver structures, as well as the analytic BER performances, of the complex QPSK communication system employed in the AWGN and flat fading channel simulations of *Chapter* 6. These baseband models were designed to be used in conjunction with the complex flat fading channel simulator shown in *Fig.* 2.5, negating the need for unnecessary carriers and subsequent high sampling frequencies during the simulations.

5.2.1 COMPLEX QPSK TRANSMITTER STRUCTURE AND OPERATION

Shown in *Fig.* 5.1 is the general structure of a baseband complex QPSK transmitter [47]. Let the m^{th} set of W antipodal coded or uncoded data bits that are to be transmitted by the complex

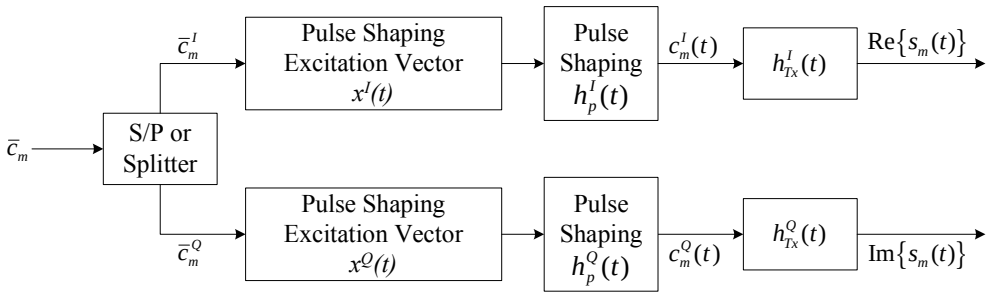

Figure 5.1: Complex QPSK Transmitter Structure

QPSK transmitter, having values from the antipodal alphabet $\{1, -1\}$, be contained in the vector $\bar{c}_m = \{c_{m,0}, c_{m,1}, ..., c_{m,W-1}\}$.

The first action taken by the transmitter is to subdivide this input data stream vector into I-channel and Q-channel symbol stream vectors according to one of two possible methods: The classic method, commonly referred to as unbalanced or dual-channel modulation, entails subdividing $\bar{c}_m$ into distinct length-$W/2$ I-channel and Q-channel symbol streams using a *serial-to-parallel* converter (denoted by the block S/P in *Fig.* 5.1). These I-channel and Q-channel symbol streams are given by:

$$\bar{c}_m^I = \{c_{m,0}^I, c_{m,1}^I, ..., c_{m,W/2-1}^I\} = \{c_{m,0}, c_{m,2}, c_{m,4}, ..., c_{m,W-2}\} \tag{5.1}$$

and:

$$\bar{c}_m^Q = \{c_{m,0}^Q, c_{m,1}^Q, ..., c_{m,W/2-1}^Q\} = \{c_{m,1}, c_{m,3}, c_{m,5}, ..., c_{m,W-1}\} \tag{5.2}$$

respectively. Note that the duration of a QPSK symbol is twice that of an uncoded data bit, i.e. $T_s = 2.T_b$.

Alternatively, the same data bits from $\bar{c}_m$ can be used on both the I-channel and the Q-channel, resulting in a *balanced* narrowband complex QPSK transmitter structure. With this transmitter configuration, the respective length-W I-channel and Q-channel symbol stream vectors are given by:

$$\bar{c}_m^I = \{c_{m,0}^I, c_{m,1}^I, ..., c_{m,W-1}^I\} = \{c_{m,0}, c_{m,1}, ..., c_{m,W-1}\} \tag{5.3}$$

and:

$$\bar{c}_m^Q = \{c_{m,0}^Q, c_{m,1}^Q, ..., c_{m,W-1}^Q\} = \{c_{m,0}, c_{m,1}, ..., c_{m,W-1}\} \tag{5.4}$$

Thus, a balanced complex QPSK transmitter is in essence a complex *Binary Phase Shift Keying* (BPSK) transmitter. The QPSK symbol rate is now the same as the bit rate, i.e. $T_s = T_b$.

Next, the antipodal I-channel and Q-channel symbols contained in these stream vectors are pulse shaped in order to minimise the transmission bandwidth and the ISI at the receiver. The first step in the pulse shaping process is to multiply the antipodal values with appropriate excitation signals for the pulse shaping filters. Since this study's narrowband complex QPSK simulations make use of square-root Nyquist pulse shaping filters (see *Section* 5.4.1), designed for impulse transmission [154], the following I-channel and Q-channel excitation signals are employed:

$$x^I(t) = x^Q(t) = \begin{cases} 1 & \text{if } t \bmod (T_p) = 0 \\ 0 & \text{Otherwise} \end{cases} \tag{5.5}$$

where $T_p = T_s$ is the duration of a QPSK symbol. Let the I-channel and Q-channel pulse shaping filters' impulse responses be denoted by $h_p^I(t)$ and $h_p^Q(t)$ (see *Section* 5.4.1), respectively. The m^{th} I-channel and Q-channel pulse shaping filter outputs are now:

$$c_m^I(t) = \left(\sum_{i=0}^{Y} c_{m,i}^I . x^I \left(t - i.T_s \right) \right) \otimes h_p^I(t) \tag{5.6}$$

and:

$$c_m^Q(t) = \left(\sum_{i=0}^{Y} c_{m,i}^Q . x^Q \left(t - i.T_s \right) \right) \otimes h_p^Q(t) \tag{5.7}$$

respectively, where $Y = W/2 - 1$ for dual-channel modulation, or $Y = W - 1$ for balanced modulation.

Further bandlimiting of the pulse shaped symbols are accomplished by the I-channel and Q-channel transmit filters, characterised by the respective impulse responses $h_{Tx}^I(t)$ and $h_{Tx}^Q(t)$. The outputs of these filters form the respective real and imaginary parts of the m^{th} output signal $s_m(t)$ of the complex QPSK transmitter:

$$s_m(t) = \text{Re}\left\{ s_m(t) \right\} + j.\,\text{Im}\left\{ s_m(t) \right\} = c_m^I(t) \otimes h_{Tx}^I(t) + j.c_m^Q(t) \otimes h_{Tx}^Q(t) \tag{5.8}$$

5.2.2 COMPLEX QPSK RECEIVER STRUCTURE AND OPERATION

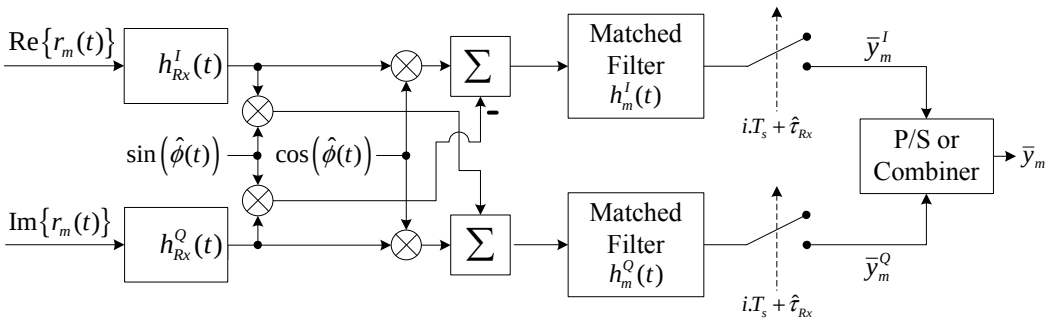

Figure 5.2: Complex QPSK Receiver Structure

The complex QPSK receiver structure [47] associated with the transmitter structure discussed in *Section* 5.2.1, is shown in *Fig.* 5.2. Assume that the m^{th} complex QPSK output signal $s_m(t)$ has been adversely effected by AWGN and flat fading channel effects, yielding the complex receiver input signal $r_m(t)$:

$$r_m(t) = \text{Re}\left\{ r_m(t) \right\} + j.\,\text{Im}\left\{ r_m(t) \right\} = \left(\text{Re}\left\{ s_m(t) \right\} + j.\,\text{Im}\left\{ s_m(t) \right\} \right) . \varpi(t) + \eta(t) \tag{5.9}$$

where $\varpi(t)$ is a complex flat fading process, defined by *Eq.* (2.46). The AWGN $\eta(t)$ is also a complex process:

$$\eta(t) = \text{Re}\left\{ \eta(t) \right\} + j.\,\text{Im}\left\{ \eta(t) \right\} \tag{5.10}$$

The complex QPSK receiver functions as follows: Firstly, the real and imaginary parts of the complex receiver input signal $r_m(t)$ are filtered by the lowpass receive filters $h_{Rx}^I(t)$ and $h_{Rx}^Q(t)$, respectively, in order to bandlimit the AWGN entering the receiver. The outputs of the receive filters are phase corrected to create the in-phase and quadrature coherent inputs for the in-phase matched filter $h_m^I(t)$ and quadrature matched filter $h_m^Q(t)$, respectively. The outputs of the in-phase and quadrature matched

filters are sampled at time instance $i.T_s + \hat{\tau}_{Rx}$ to give:

$$y^I_{m,i} = \Big[\Big(\big[h^I_{Rx}(t) \otimes \mathrm{Re}\{r_m(t)\}\big] \cos\Big(\hat{\phi}(t)\Big) - \Big[h^Q_{Rx}(t) \otimes \mathrm{Im}\{r_m(t)\}\Big] \sin\Big(\hat{\phi}(t)\Big)\Big) \otimes h^I_m(t)\Big]_{t=i.T_s+\hat{\tau}_{Rx}} \tag{5.11}$$

and:

$$y^Q_{m,i} = \Big[\Big(\Big[h^Q_{Rx}(t) \otimes \mathrm{Im}\{r_m(t)\}\Big] \sin\Big(\hat{\phi}(t)\Big) + \big[h^I_{Rx}(t) \otimes \mathrm{Re}\{r_m(t)\}\big] \cos\Big(\hat{\phi}(t)\Big)\Big) \otimes h^Q_m(t)\Big]_{t=i.T_s+\hat{\tau}_{Rx}} \tag{5.12}$$

respectively, where $\hat{\phi}(t)$ is the sum of an estimate of the channel phase alteration experienced by the transmitted signal (see *Section* 3.3.5) and the phase distortion introduced by the receive filters. The parameter $\hat{\tau}_{Rx}$ is an estimate of the time delay a complex QPSK symbol experiences due to the receive filters. These sampled matched filter outputs are then stored in the vectors $\overline{y}^I_m = \{y^I_{m,0}, y^I_{m,1}, ..., y^I_{m,W/2-1}\}$ and $\overline{y}^Q_m = \{y^Q_{m,0}, y^Q_{m,1}, ..., y^Q_{m,W/2-1}\}$, respectively.

The final action taken by the complex QPSK receiver is to create the resultant receiver output vector $\overline{y}_m$, which is an estimate of the original data bit vector $\overline{c}_m$ used by the transmitter as input (see *Section* 5.2.1): For dual-channel modulation, $\overline{y}_m$ is constructed by interweaving the m^{th} I-channel and Q-channel estimate vectors using a *parallel-to-serial* converter (denoted by the block P/S in *Fig.* 5.2), whereas with balanced modulation, $\overline{y}^I_m$ and $\overline{y}^Q_m$ are linearly combined to form $\overline{y}_m$.

5.2.3 AVERAGE FADING AMPLITUDE CALCULATION FOR COMPLEX QPSK SYSTEMS

Calculation of the average fading amplitude, associated with each output estimate contained in the vector $\overline{y}_m$, is accomplished by filtering an estimate of the instantaneous fading amplitude using an averaging filter $h_{ave}(t)$ which has an impulse response identical to the matched filters used in *Fig.* 5.2. Extraction of the average fading amplitude from this filter differs for balanced and unbalanced transmitter configurations: With balanced modulation the i^{th} symbols transmitted on the I-channel and Q-channel are identical. Hence, an estimate of the average fading amplitude associated with the i^{th} element in $\overline{y}_m$ is determined as follows:

$$\hat{\overline{\alpha}}_{m,i} = [\hat{\alpha}(t) \otimes h_{ave}(t)]_{t=i.T_s+\hat{\tau}_{Rx}} \tag{5.13}$$

where $\hat{\alpha}(t)$ represents an estimate of the instantaneous fading amplitude, as described by *Eq.* (2.9) for the trivial case of a single path multipath channel. Considering dual-channel modulation, recall from *Section* 5.2.1 that the i^{th} I-channel and Q-channel symbols are transmitted simultaneously. Therefore, it is apparent that they will experience the same instantaneous amplitude fading (see *Section* 2.4.1). Hence, an estimate of the average fading amplitudes associated with the $(2.i)^{\text{th}}$ and $(2.i+1)^{\text{th}}$ elements in the output vector $\overline{y}_m$ is obtained as follows:

$$\hat{\overline{\alpha}}_{m,(2.i)} = \hat{\overline{\alpha}}_{m,(2.i+1)} = [\hat{\alpha}(t) \otimes h_{ave}(t)]_{t=(2.i).T_s+\hat{\tau}_{Rx}} \tag{5.14}$$

5.2.4 ANALYTICAL BIT ERROR PROBABILITIES OF UNCODED NARROWBAND COMPLEX QPSK COMMUNICATION SYSTEMS

5.2.4.1 AWGN CHANNEL CONDITIONS

Assuming coherent demodulation, it can be shown that the symbol error probability for a dual-channel QPSK system functioning in AWGN channel (see *Section* 2.2) conditions is given by [81]:

$$P_s\left(e\right) = 2Q\left(\sqrt{\gamma_{s,m,i}}\right) - \frac{1}{2}\left[Q\left(\sqrt{\gamma_{s,m,i}}\right)\right]^2 \tag{5.15}$$

where $Q(\,.\,)$ denotes the Q-function [47]. The SNR per QPSK symbol for the i^{th} symbol in the m^{th} set of symbols, denoted by $\gamma_{s,m,i}$, is defined as follows:

$$\gamma_{s,m,i} = \frac{E_s}{N_0} \tag{5.16}$$

where E_s is the energy per transmitted symbol and N_0 is the single sided PSD of the AWGN. Note that the squared term in *Eq.* (5.15) becomes negligible if $\gamma_{s,m,i}/2 >> 1$ [81]. Thus, it is commonplace to approximate *Eq.* (5.15) with:

$$P_s\left(e\right) \simeq 2Q\left(\sqrt{\gamma_{s,m,i}}\right) \tag{5.17}$$

Recall that two data bits are transmitted per symbol in an uncoded dual-channel narrowband QPSK system. Hence, the energy per bit is simply $E_b = E_s/2$ [J]. Thus, employing Gray mapping of bits to QPSK symbols, the bit error probability of such a system can be approximated by [81]:

$$P_b\left(e\right) = \left.\frac{P_s\left(\gamma_{s,m,i}\right)}{2}\right|_{\gamma_{s,m,i}=2.\gamma_{b,m,i}} \simeq Q\left(\sqrt{2.\gamma_{b,m,i}}\right) \tag{5.18}$$

where $\gamma_{b,m,i}$ is the SNR per bit for the i^{th} bit in the m^{th} vector of data bits, given by:

$$\gamma_{b,m,i} = \frac{E_b}{N_0} \tag{5.19}$$

In *Section* 5.2.1 it is stated that a QPSK transmitter configured for balanced modulation is essentially a BPSK transmitter. Thus, the bit error probability for a balanced QPSK communication system in AWGN channel conditions will be given by [81]:

$$P_b\left(e\right) = Q\left(\sqrt{2.\gamma_{b,m,i}}\right) = Q\left(\sqrt{\frac{2E_b}{N_0}}\right) \tag{5.20}$$

where *Eq.* (5.19) remains valid. Thus, the BER for balanced and unbalanced narrowband QPSK systems are essentially the same.

5.2.4.2 SLOW RAYLEIGH FLAT FADING CHANNEL CONDITIONS

Assume a narrowband QPSK signal (balanced or unbalanced) is transmitted through a slow (see *Section* 2.5.1.2) Rayleigh (see *Section* 2.5.2.1) flat fading (see *Section* 2.5.1.1) channel. If the multiplicative fading process is slow enough that the Rayleigh distributed fading amplitude may be regarded as a constant during at least one symbol interval, i.e. $\alpha_{m,i}(t) = \overline{\alpha}_{m,i}$ for the i^{th} bit in the m^{th} message bit vector, the system's SNR per bit is given by [47, 152]:

$$\gamma_{b,m,i} = \overline{\alpha}_{m,i}^2 \frac{E_b}{N_0} \tag{5.21}$$

The $\overline{\alpha}_{m,i}^2$ is time-invariant with a *chi-squared* PDF with two degrees of freedom. Hence, $\gamma_{b,m,i}$ is a stochastic variable, which also has a chi-squared PDF with two degrees of freedom, given by [47,152]:

$$\rho\left(\gamma_{b,m,i}\right) = \frac{1}{\overline{\gamma}_{b,m,i}} \exp\left(-\frac{\gamma_{b,m,i}}{\overline{\gamma}_{b,m,i}}\right) \qquad \text{for } \gamma_{b,m,i} \geqslant 0 \tag{5.22}$$

where $\overline{\gamma}_{b,m,i}$ is the average SNR per bit, given by [47, 152]:

$$\overline{\gamma}_{b,m,i} = E\left[\overline{\alpha}_{m,i}^2\right] \frac{E_b}{N_0} = \frac{\overline{E}_b}{N_0} \tag{5.23}$$

In this equation $\overline{E}_b$ is the average energy per bit and $E[\,.\,]$ denotes expectation. Since the derivation of the bit error probabilities of *Eq.* (5.18) and *Eq.* (5.20) were done for non-faded channel conditions, i.e. $\overline{\alpha}_{m,i} = 1$, these equations can be viewed as conditional error probabilities, with the condition that $\overline{\alpha}_{m,i}$ remains fixed. Therefore, obtaining the average bit error probability for balanced and unbalanced narrowband QPSK systems when $\overline{\alpha}_{m,i}$ is random, necessitates averaging $P_b\left(e|\gamma_{b,m,i}\right)$ over the PDF of $\gamma_{b,m,i}$ [47, 152]:

$$\begin{aligned} P_b\left(e\right) &= \int_0^\infty P_b\left(e|\gamma_{b,m,i}\right) \rho\left(\gamma_{b,m,i}\right) d\gamma_{b,m,i} \\ &= \frac{1}{2}\left(1 - \sqrt{\frac{\overline{\gamma}_{b,m,i}}{1+\overline{\gamma}_{b,m,i}}}\right) \\ &= \frac{1}{2}\left(1 - \sqrt{\frac{\frac{\overline{E}_b}{N_0}}{1+\frac{\overline{E}_b}{N_0}}}\right) \end{aligned} \tag{5.24}$$

5.3 RAKE RECEIVER-BASED COMPLEX DS/SSMA QPSK COMMUNICATION SYSTEMS

In the following subsections the RAKE receiver-based complex DS/SSMA QPSK communication system, employed in the multipath fading channel simulations of *Chapter* 6, is presented. Thorough descriptions of the transmitter and receiver structures are followed by a theoretical BER performance analysis of the system. The complex transmitter and receiver models presented here were designed to be used in conjunction with the complex multipath fading channel simulator shown in *Fig.* 2.8, once again negating the need for unnecessary carriers and subsequent high simulation sampling frequencies.

5.3.1 COMPLEX DS/SSMA QPSK TRANSMITTER STRUCTURE AND OPERATION

Fig. 5.3 depicts the generic structure of the baseband complex DS/SSMA QPSK transmitter of user-q in a multi-user CDMA system [43, 47]. Assume that the m^{th} input to this transmitter is $\overline{c}_m^q = \{c_{m,0}^q, c_{m,1}^q, ..., c_{m,W-1}^q\}$, which is a vector containing W antipodal bits with values from the alphabet $\{1, -1\}$. As shown in *Fig.* 5.3, two options are available for the initial processing of this vector of data bits: The first option is to subdivide it using a serial-to-parallel converter (denoted by the block S/P in *Fig.* 5.3) into distinct I-channel and Q-channel symbol stream vectors, given by:

$$\overline{c}_m^{I,q} = \{c_{m,0}^{I,q}, c_{m,1}^{I,q}, ..., c_{m,W/2-1}^{I,q}\} = \{c_{m,0}^q, c_{m,2}^q, c_{m,4}^q, ..., c_{m,W-2}^q\} \tag{5.25}$$

and

$$\overline{c}_m^{Q,q} = \{c_{m,0}^{Q,q}, c_{m,1}^{Q,q}, ..., c_{m,W/2-1}^{Q,q}\} = \{c_{m,1}^q, c_{m,3}^q, c_{m,5}^q, ..., c_{m,W-1}^q\} \tag{5.26}$$

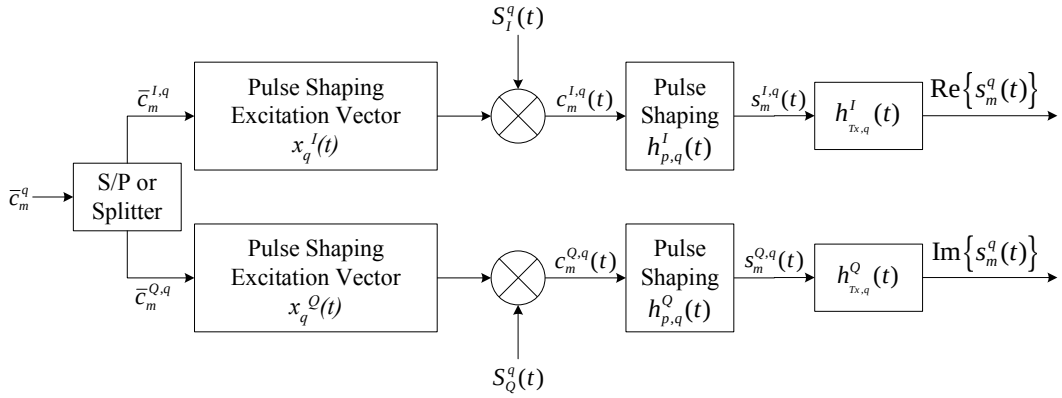

Figure 5.3: Complex DS/SSMA QPSK Transmitter Structure

respectively. This approach is frequently used when binary spreading sequences are employed in the DS/SSMA QPSK system. The symbol rate of the transmitter is half the uncoded bit rate, i.e. $T_s = 2.T_b$.

The second option is to use the same data bits on both the I-channel and Q-channel, creating a *balanced* complex DS/SSMA QPSK transmitter structure [43, 46, 50, 51] with length-W I-channel and Q-channel symbols stream vectors, given by:

$$\bar{c}_m^{I,q} = \{c_{m,0}^{I,q}, c_{m,1}^{I,q}, ..., c_{m,W-1}^{I,q}\} = \{c_{m,0}^{q}, c_{m,1}^{q}, ..., c_{m,W-1}^{q}\} \tag{5.27}$$

and

$$\bar{c}_m^{Q,q} = \{c_{m,0}^{Q,q}, c_{m,1}^{Q,q}, ..., c_{m,W-1}^{Q,q}\} = \{c_{m,0}^{q}, c_{m,1}^{q}, ..., c_{m,W-1}^{q}\} \tag{5.28}$$

respectively. This transmitter configuration, where the symbol and bit rates are equivalent, is frequently used in DS/SSMA QPSK systems employing pre-filtered CSSs (see *Section* D.3.2) in order to take full advantage of the spectral characteristics of the CSSs (see *Section* 6.4.3). For example, in [7, 10] such a balanced transmitter structure is employed in conjunction with ABC sequences (see *Section* D.3.2.2) to deliver SSB transmitter output signals.

The antipodal values contained in the I-channel and Q-channel symbol stream vectors are now pulse shaped. This is accomplished by first multiplying these symbols with appropriate pulse shaping excitation signals. Excitation vectors similar to those given in *Eq.* (5.5) are used, with $T_p = T_{chip}$ (the duration of a CSS chip). Square-root Nyquist pulse shaping filters (see *Section* 5.4.1), designed for impulse transmission, are used in *Chapter* 6's DS/SSMA simulations that employ unfiltered CSSs (see *Section* D.3.1). Alternatively, the simulations presented in this study that make use of filtered CSSs (see *Section* D.3.2) employ no additional pulse shaping, hence the following I-channel and Q-channel chip-level pulse shaping filter impulse responses are used in user-q's transmitter:

$$h_{p,q}^I(t) = h_{p,q}^Q(t) = \begin{cases} 1 & \text{for } 0 < t \leq T_{chip} \\ 0 & \text{Otherwise} \end{cases} \tag{5.29}$$

After multiplication with the excitation signals, the I-channel and Q-channel are spreaded with user-q's I-channel and Q-channel spreading sequences, denoted by $S_I^q(t)$ and $S_Q^q(t)$, respectively. These spreading sequences are unique to user-q. When CSSs are employed in the CDMA system, $S_I^q(t)$ and $S_Q^q(t)$ can be the real and imaginary parts of user-q's unique CSS (see *Section* D.3.1), respectively [50, 51]. Another possibility is that $S_I^q(t)$ and $S_Q^q(t)$ may be linear combinations of the real and

imaginary parts of the CSS [155]. In this study the former approach was employed, i.e. $S_I^q(t) = \mathrm{Re}\{S^q(t)\}$ and $S_Q^q(t) = \mathrm{Im}\{S^q(t)\}$. The resultant spreaded I-channel and Q-channel streams are given by:

$$c_m^{I,q}(t) = \sum_{j=0}^{Y} c_{m,j}^{I,q}.x_q^I(t - j.T_s).S_I^q(t) \tag{5.30}$$

and:

$$c_m^{Q,q}(t) = \sum_{j=0}^{Y} c_{m,j}^{Q,q}.x_q^Q(t - j.T_s).S_Q^q(t) \tag{5.31}$$

respectively, where $Y = W - 1$ or $Y = W/2 - 1$ for balanced or unbalanced (dual-channel) transmitter structures, respectively. In *Eq.* (5.30) and *Eq.* (5.31), T_s [s] is the symbol duration. The actual pulse shaping of the spreaded I-channel and Q-channel information are now accomplished using user-q's in-phase and quadrature pulse shaping filters, characterised by the impulse responses $h_{p,q}^I(t)$ and $h_{p,q}^Q(t)$, respectively. The resultant I-channel and Q-channel spreaded pulse shaped symbols are given by:

$$s_m^{I,q}(t) = c_m^{I,q}(t) \otimes h_{p,q}^I(t) \tag{5.32}$$

and:

$$s_m^{Q,q}(t) = c_m^{Q,q}(t) \otimes h_{p,q}^Q(t) \tag{5.33}$$

respectively, where $\otimes$ denotes convolution.

Lastly, the in-phase and quadrature pulse shaped symbol streams are bandlimited by the transmit filters $h_{Tx,q}^I(t)$ and $h_{Tx,q}^Q(t)$, respectively, to give user-q's complex DS/SSMA QPSK transmitter output signal:

$$\begin{aligned} s_m^q(t) &= \mathrm{Re}\{s_m^q(t)\} + j.\,\mathrm{Im}\{s_m^q(t)\} \\ &= s_m^{I,q}(t) \otimes h_{Tx,q}^I(t) + j.s_m^{Q,q}(t) \otimes h_{Tx,q}^Q(t) \end{aligned} \tag{5.34}$$

5.3.2 COMPLEX DS/SSMA QPSK RAKE RECEIVER STRUCTURE AND OPERATION

Assume that user-q's m^{th} complex DS/SSMA QPSK transmitter output signal traverses a time-invariant discrete multipath fading channel (see *Section* 2.4.1), consisting of L^q statistically independent flat fading (see *Section* 2.5.1.1) paths [156]. The average path gain and delay associated with this multipath channel's i^{th} path, for $i = 1, 2, ..., L^q$, are $\overline{\beta}_i^q$ and τ_i^q, respectively. Note that the complex input to user-q's receiver, denoted by $r_m^q(t)$, will consist not only of a distorted version of the signal generated by user-q's transmitter, but also distorted signals originating from the transmitters of the other users in the CDMA system.

Since a multipath fading channel exhibits a tapped delay line nature, it is apparent that the receiver is provided with L^q scaled replicas of the same transmitted signal, each replica experiencing flat fading, which is hopefully statistically independent from that experienced by the other replicas [47, 110]. Hence, a receiver that is capable of optimally processing the received signal, collecting the signal energy contained within each of the received multipath components, will achieve the performance of an equivalent L^q-th order diversity communication system. In 1958 *Price* and *Green* [157] proposed such a receiver structure for which the name "RAKE receiver" has been coined, since its energy accumulation action is somewhat analogous to an ordinary garden rake. *Fig.* 5.4 depicts the RAKE receiver structure [43, 47], capable of optimally processing user-q's complex received signal [158].

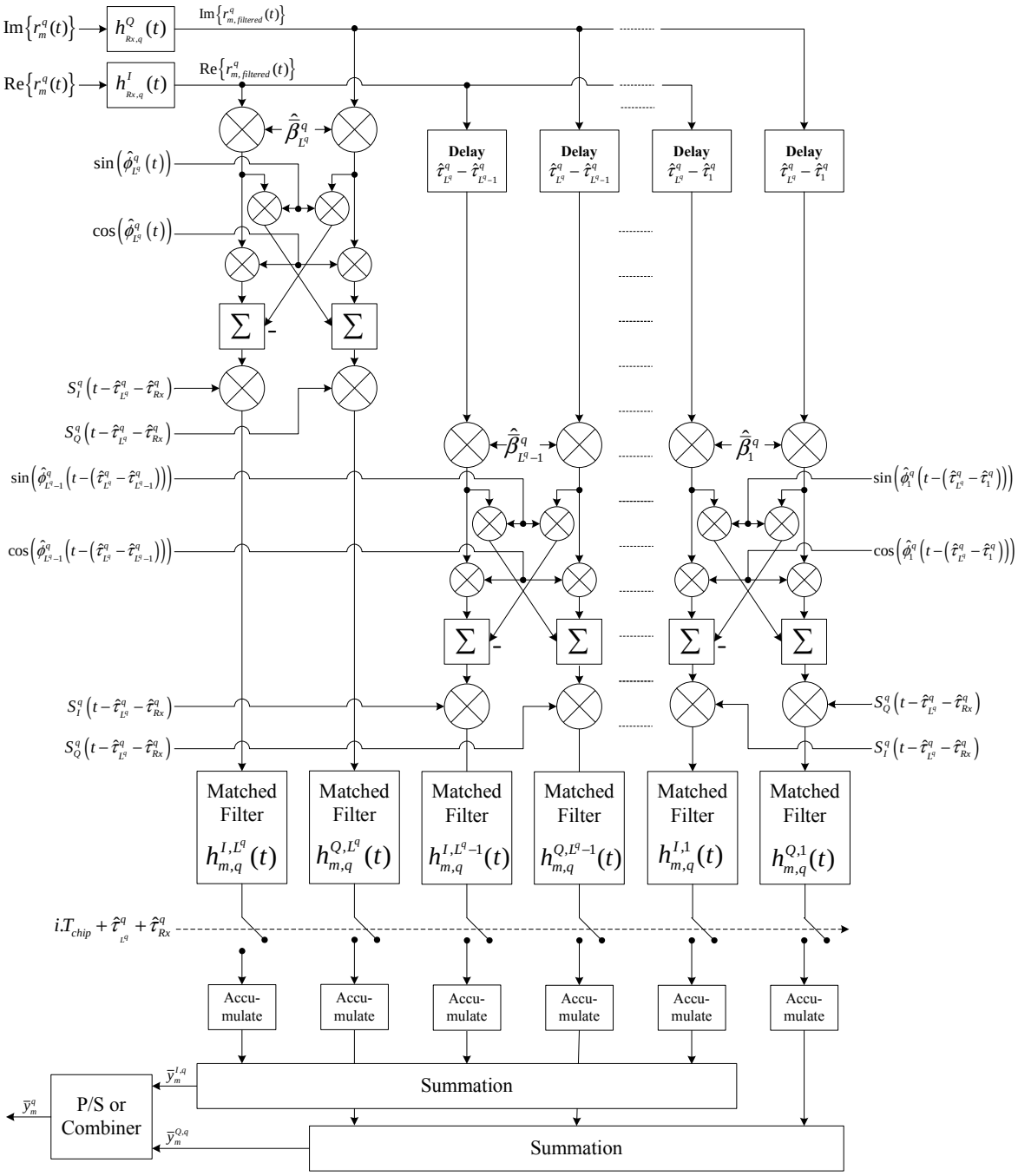

Figure 5.4: Complex DS/SSMA QPSK RAKE Receiver Structure

The first step in the demodulation process is to bandlimit the AWGN present in the complex received signal $r_m^q(t)$ using the I-channel lowpass receive filter $h_{Rx,q}^I(t)$ and Q-channel lowpass receive filter $h_{Rx,q}^Q(t)$. The resultant filtered complex received signal is given by:

$$\begin{aligned} r_{m,filtered}^q(t) &= \mathrm{Re}\left\{r_{m,filtered}^q(t)\right\} + j.\,\mathrm{Im}\left\{r_{m,filtered}^q(t)\right\} \\ &= \mathrm{Re}\left\{r_m^q(t)\right\} \otimes h_{Rx,q}^I(t) + j.\,\mathrm{Im}\left\{r_m^q(t)\right\} \otimes h_{Rx,q}^Q(t) \end{aligned} \tag{5.35}$$

Next, the noisy flat faded L^q received delayed versions of user-q's m^{th} original complex transmitted signal are realigned with the last received multipath component. This is accomplished by creating L^q delayed versions of the signal $r_{m,filtered}^q(t)$, namely $r_{m,filtered}^q\left(t-\left(\hat{\tau}_{L^q}^q-\hat{\tau}_i^q\right)\right)$, with $i=1,2,...,L^q$. The term $\hat{\tau}_i^q$ is an estimate of the path delay of the i^{th} multipath component. In order for the RAKE receiver to function optimally, it requires perfect knowledge of the path delay of each of the multipath components, i.e. $\hat{\tau}_i^q=\tau_i^q$ for $i=1,2,...,L^q$ (see *Section* 3.3.5).

Since the multipath components arriving at the receiver have experienced statistically independent flat fading and attenuation, as dictated by the power delay profile of user-q's multipath fading channel (see *Section* 2.4.2), each received component's contribution to the total realigned m^{th} complex received signal varies. In order to increase the influence of strong multipath components and decrease the influence of weak multipath components, each of the delayed complex received signal versions is scaled, prior to demodulation, with an estimate (see *Section* 3.3.5) of its average envelope amplitude (see *Section* 2.4.1). For example, the delayed filtered complex received signal $r_{m,filtered}^q\left(t-\left(\hat{\tau}_{L^q}^q-\hat{\tau}_i^q\right)\right)$ is scaled by the average envelope amplitude estimate $\hat{\overline{\beta}}_i^q$. The use of this scaling technique is commonly referred to as MRC [43, 47, 152]. Other popular RAKE combining techniques are *Equal Gain Combining* (EGC) and *Differential Phase Combining* (DPC) [158]. Optimal MRC processing of the complex received signal only occurs if the receiver has perfect knowledge of the average envelope amplitude of each of the multipath components, i.e. $\hat{\overline{\beta}}_i^q=\overline{\beta}_i^q$ for $i=1,2,...,L^q$.

Next, the receiver phase corrects each of the scaled and delayed versions of the m^{th} filtered complex received signal. For the i^{th} delayed, scaled and filtered complex received signal component $\hat{\overline{\beta}}_i^q.r_{m,filtered}^q\left(t-\left(\hat{\tau}_{L^q}^q-\hat{\tau}_i^q\right)\right)$, this is accomplished by mixing it with the complex exponent $\exp\left(-j.\hat{\phi}_i^q\left(t-\left(\hat{\tau}_{L^q}-\hat{\tau}_i^q\right)\right)\right)$. The instantaneous phase $\hat{\phi}_i^q\left(t-\left(\hat{\tau}_{L^q}-\hat{\tau}_i^q\right)\right)$ is an estimate (see *Section* 3.3.5) of the channel phase changes experienced by the i^{th} complex received multipath component at the time of its reception, as well as phase distortion added by the I-channel and Q-channel receive filters. Coherent demodulation takes place in the event that the receiver has perfect knowledge of the path delays, I-channel and Q-channel receive filter phase distortions and each of the multipath component's channel phase [86], i.e. $\hat{\phi}_i^q\left(t-\left(\hat{\tau}_{L^q}-\hat{\tau}_i^q\right)\right)=\phi_i^q\left(t-\left(\tau_{L^q}-\tau_i^q\right)\right)$ for $i=1,2,...,L^q$.

In order to despread user-q's m^{th} complex received signal, each of the L^q phase corrected I-channel and Q-channel signals are respreaded with delayed versions of user-q's I-channel and Q-channel spreading sequences, $S_I^q\left(t-\hat{\tau}_{L^q}^q-\hat{\tau}_{Rx}^q\right)$ and $S_Q^q\left(t-\hat{\tau}_{L^q}^q-\hat{\tau}_{Rx}^q\right)$, respectively. The time delays $\hat{\tau}_{L^q}^q$ and $\hat{\tau}_{Rx}^q$ introduced into the spreading sequences are estimates of the total delay experienced by the realigned set of complex received signals and the time delay introduced by the receive filters, respectively. Despreading is completely successful only if the receiver has perfect knowledge of these time delays.

Continuing the demodulation procedure, the I-channel and Q-channel despreaded signals of the i^{th} RAKE receiver tap are now processed by the respective matched filters, $h_{m,q}^{I,i}(t)$ and $h_{m,q}^{Q,i}(t)$. These

filters are matched to the chip-level pulse shaping filters employed in the DS/SSMA QPSK transmitter. The outputs of the L^q I-channel and Q-channel matched filters are sampled at time instances $t = a.T_{chip} + \hat{\tau}^q_{L^q} + \hat{\tau}^q_{Rx}$, with T_{chip} the duration of a spreading sequence chip. Each of the I-channel and Q-channel matched filter outputs are accumulated for a duration of T_s [s], whereafter the accumulated values are normalised with respect to T_s/T_{chip}. The L^q I-channel accumulated values are then linearly combined to give an estimate of the j^{th} symbol in the original transmitted I-channel symbol vector $\overline{c}^{I,q}_m$, created by the DS/SSMA QPSK transmitter:

$$\begin{aligned} y^{I,q}_{m,j} = & \frac{T_{chip}}{T_s} \sum_{i=1}^{L^q} \sum_{a=1}^{T_s/T_{chip}} \left[\left(\hat{\overline{\beta}}^q_i \left[\text{Re} \left\{ r^q_{m,filtered} \left(t - \left(\hat{\tau}^q_{L^q} - \hat{\tau}^q_i \right) \right) \right\} . \cos \left(\hat{\phi}^q_i \left(t - \left(\hat{\tau}_{L^q} - \hat{\tau}^q_i \right) \right) \right) - \right. \right. \right. \\ & \left. \left. \left. \text{Im} \left\{ r^q_{m,filtered} \left(t - \left(\hat{\tau}^q_{L^q} - \hat{\tau}^q_i \right) \right) \right\} . \sin \left(\hat{\phi}^q_i \left(t - \left(\hat{\tau}_{L^q} - \hat{\tau}^q_i \right) \right) \right) \right] \times \right. \\ & \left. S^q_I \left(t - \hat{\tau}^q_{L^q} - \hat{\tau}^q_{Rx} \right) \right) \otimes h^{I,i}_{m,q}(t) \Big]_{t = j.T_s + a.T_{chip} + \hat{\tau}^q_{L^q} + \hat{\tau}^q_{Rx}} \end{aligned} \tag{5.36}$$

Linearly combining the normalised L^q Q-channel accumulated values results in an estimate of the j^{th} symbol of the original transmitted Q-channel symbol vector $\overline{c}^{Q,q}_m$:

$$\begin{aligned} y^{Q,q}_{m,j} = & \frac{T_{chip}}{T_s} \sum_{i=1}^{L^q} \sum_{a=1}^{T_s/T_{chip}} \left[\left(\hat{\overline{\beta}}^q_i \left[\text{Im} \left\{ r^q_{m,filtered} \left(t - \left(\hat{\tau}^q_{L^q} - \hat{\tau}^q_i \right) \right) \right\} . \sin \left(\hat{\phi}^q_i \left(t - \left(\hat{\tau}_{L^q} - \hat{\tau}^q_i \right) \right) \right) + \right. \right. \right. \\ & \left. \left. \left. \text{Re} \left\{ r^q_{m,filtered} \left(t - \left(\hat{\tau}^q_{L^q} - \hat{\tau}^q_i \right) \right) \right\} . \cos \left(\hat{\phi}^q_i \left(t - \left(\hat{\tau}_{L^q} - \hat{\tau}^q_i \right) \right) \right) \right] \times \right. \\ & \left. S^q_Q \left(t - \hat{\tau}^q_{L^q} - \hat{\tau}^q_{Rx} \right) \right) \otimes h^{Q,i}_{m,q}(t) \Big]_{t = j.T_s + a.T_{chip} + \hat{\tau}^q_{L^q} + \hat{\tau}^q_{Rx}} \end{aligned} \tag{5.37}$$

Finalising the demodulation process, user-q's DS/SSMA QPSK RAKE receiver creates the output vector $\overline{y}^q_m$, which is an estimate of the original DS/SSMA QPSK transmitter input vector $\overline{c}^q_m$. This is accomplished by one of two possible methods: If the transmitter structure is configured for balanced modulation, $\overline{y}^q_m$ is constructed by linearly combining the elements from $\overline{y}^{I,q}_m$ and $\overline{y}^{Q,q}_m$. Alternatively, a *parallel-to-serial* converter (denoted by the block P/S in *Fig.* 5.4) creates $\overline{y}^q_m$ by interlacing the elements of $\overline{y}^{I,q}_m$ and $\overline{y}^{Q,q}_m$.

5.3.3 AVERAGE OUTPUT FADING AMPLITUDE CALCULATION FOR COMPLEX DS/SSMA QPSK SYSTEMS WITH RAKE RECEIVERS

The first step in the calculation of user-q's average fading amplitude for the i^{th} multipath fading channel component is to delay an estimate of its instantaneous fading amplitude $\hat{\alpha}^q_i(t)$ by $\left(\hat{\tau}^q_{L^q} - \hat{\tau}^q_i \right)$. Next, this delayed estimate of the i^{th} channel component's instantaneous fading amplitude is filtered using an averaging filter $h^i_{ave,q}(t)$, which has an impulse response identical to the matched filters used in *Fig.* 5.4. Recall that the delayed complex received signal $r^q_{m,filtered} \left(t - \left(\hat{\tau}^q_{L^q} - \hat{\tau}^q_i \right) \right)$, with $i = 1, 2, ..., L^q$, is scaled by the average envelope amplitude estimate $\hat{\overline{\beta}}^q_i$ during MRC. Hence, the average fading amplitudes associated with the elements in the receiver output vector $\overline{y}^q_m$ are normalised averages of the linear combination of the delayed average fading amplitudes experienced by each of the multipath components. However, the calculation thereof differs for the balanced and unbalanced DS/SSMA QPSK communication system configurations in *Fig.* 5.3 and *Fig.* 5.4: For the balanced modulation scenario, the same data bits are transmitted on the I-channel and Q-channel. Hence, calculation of an estimate of the average fading amplitude associated with the j^{th} element of user-q's

receiver output vector $\overline{y}_m^q$, is accomplished as follows:

$$\hat{\overline{\alpha}}_{m,j}^q = \frac{T_{chip}}{T_s} \sum_{i=1}^{L^q} \sum_{a=1}^{T_s/T_{chip}} \hat{\overline{\beta}}_i^q \left[\hat{\alpha}_i^q \left(t - \left(\hat{\tau}_{L^q}^q - \hat{\tau}_i^q \right) \right) \otimes h_{ave,q}^i(t) \right]_{t=j.T_s+a.T_{chip}+\hat{\tau}_{L^q}^q+\hat{\tau}_{Rx}^q} \tag{5.38}$$

where $\hat{\overline{\beta}}_i^q$ and $\hat{\tau}_i^q$ are estimates of the i^{th} multipath component's average envelope amplitude (see *Section* 2.4.1) and delay, respectively. In the case of dual-channel modulation, the j^{th} set of symbols that are transmitted on the I-channel and Q-channel are two consecutive data bits from the transmitter input vector $\overline{c}_m^q$, defined in *Section* 5.3.1. Consequently, an estimate of the average fading amplitude associated with the $(2.j)^{\text{th}}$ and $(2.j+1)^{\text{th}}$ elements of user-q's receiver output vector $\overline{y}_m^q$, can be calculated as follows:

$$\begin{aligned} \hat{\overline{\alpha}}_{m,(2.j)}^q &= \hat{\overline{\alpha}}_{m,(2.j+1)}^q \\ &= \frac{T_{chip}}{T_s} \sum_{i=1}^{L^q} \sum_{a=1}^{T_s/T_{chip}} \hat{\overline{\beta}}_i^q \left[\hat{\alpha}_i^q \left(t - \left(\hat{\tau}_{L^q}^q - \hat{\tau}_i^q \right) \right) \otimes h_{ave,q}^i(t) \right]_{t=(2.j).T_s+a.T_{chip}+\hat{\tau}_{L^q}^q+\hat{\tau}_{Rx}^q} \end{aligned} \tag{5.39}$$

5.3.4 ANALYTICAL BIT ERROR PROBABILITY FOR SINGLE USER DS/SSMA QPSK SYSTEMS WITH RAKE RECEIVERS

In [47] an approximate bit error probability is derived for the RAKE receiver-based DS/SSMA QPSK system discussed in the previous subsections. The derivation is made under the following assumptions:

- User-q is the only user present in the CDMA system. Consequently, MUI is absent from the communication system.
- The periodic auto-correlation (see *Section* D.2.2) of user-q's I-channel and Q-channel spreading sequences is perfect, i.e.:

$$R_{S_I^q(t),S_I^q(t)}(\tau) = R_{S_Q^q(t),S_Q^q(t)}(\tau) = \delta(\tau) \tag{5.40}$$

- The periodic cross-correlation (see *Section* D.2.3) between user-q's I-channel and Q-channel spreading sequences is perfect, i.e.:

$$R_{S_I^q(t),S_Q^q(t)}(\tau) = 0 \qquad \forall \tau \tag{5.41}$$

- Slow Rayleigh (see *Section* 2.5.2.1) flat fading (see *Section* 2.5.1.1) is experienced by each of the L^q statistically independent paths of user-q's multipath fading channel.
- User-q's DS/SSMA QPSK RAKE receiver has perfect knowledge of the instantaneous phase, delay and envelope amplitude CSI parameters of each of the L^q paths in the multipath fading channel.

Derivation of the bit error probability, valid for both balanced and unbalanced modulation, is accomplished by first recognising that the conditional probability of error for user-q's RAKE receiver-based DS/SSMA QPSK system is given by [47]:

$$P_b^q\left(e|\gamma_{b,m,j}^q\right) = Q\left(\sqrt{2.\gamma_{b,m,j}^q}\right) \tag{5.42}$$

where $\gamma^q_{b,m,j}$ is user-q's total received SNR per bit for the j^{th} bit in the m^{th} vector of data bits. Thus, user-q's bit error probability $P^q_b(e)$ can obtained by averaging $P^q_b\left(e|\gamma^q_{b,m,j}\right)$ over the PDF of the total SNR per bit, denoted by $\rho\left(\gamma^q_{b,m,j}\right)$: If the flat fading experienced by each of the L^q paths is slow enough that the Rayleigh distributed fading amplitude may be regarded as a constant (during at least one symbol interval), i.e. $\beta^q_i(t) = \overline{\beta}^q_i$ for $i = 1, 2, ..., L^q$, it can be shown that the SNR per bit for the j^{th} bit in the m^{th} vector of data bits of user-q's i^{th} received multipath component is given by:

$$\gamma^{q,i}_{b,m,j} = \left(\overline{\beta}^q_i\right)^2 \frac{\overline{E}^q_b}{N_0} \tag{5.43}$$

where $\overline{E}^q_b$ is user-q's average transmitted energy per bit. It is worthwhile to note that the energy per bit for balanced and unbalanced modulation is identical for the transmitter structure shown in *Fig.* 5.3 [50]. Thus, user-q's total received SNR per bit for the j^{th} bit in the m^{th} message word can be calculated as follows:

$$\gamma^q_{b,m,j} = \sum_{i=1}^{L^q} \gamma^{q,i}_{b,m,j} = \frac{\overline{E}^q_b}{N_0} \sum_{i=1}^{L^q} \left(\overline{\beta}^q_i\right)^2 \tag{5.44}$$

Since $\gamma^{q,i}_{b,m,j}$, with $i = 1, 2, ..., L^q$, are random variables with chi-squared distributions (with two degrees of freedom), it can be shown that the PDF of the total SNR per bit is given by [47, 152]:

$$\rho\left(\gamma^q_{b,m,j}\right) = \sum_{i=1}^{L^q} \left[\frac{1}{\overline{\gamma}^{q,i}_{b,m,j}} \left(\prod_{a=1, a\neq i}^{L^q} \frac{\overline{\gamma}^{q,i}_{b,m,j}}{\overline{\gamma}^{q,i}_{b,m,j} - \overline{\gamma}^{q,a}_{b,m,j}} \right) \exp\left(-\frac{\gamma^q_{b,m,j}}{\overline{\gamma}^{q,i}_{b,m,j}} \right) \right] \qquad \text{for } \gamma^q_{b,m,j} \geq 0 \tag{5.45}$$

where $\overline{\gamma}^{q,i}_{bm,j}$ is the average SNR per bit for the j^{th} bit in the m^{th} message word vector on the i^{th} path, defined as:

$$\overline{\gamma}^{q,i}_{b,m,j} = E\left[\left(\overline{\beta}^q_i\right)^2\right] \frac{E^q_b}{N_0} \tag{5.46}$$

with $E[\ .\ ]$ denoting expectancy. Thus, with $\rho\left(\gamma^q_{b,m,j}\right)$ as defined by *Eq.* (5.45), the bit error probability for user-q can be determined as follows [47, 152]:

$$\begin{aligned} P^q_b(e) &= \int_0^\infty P^q_b\left(e|\gamma^q_{b,m,j}\right) \rho\left(\gamma^q_{b,m,j}\right) d\gamma^q_{b,m,j} \\ &= \frac{1}{2} \sum_{i=1}^{L^q} \left[\left(\prod_{a=1, a\neq i}^{L^q} \frac{\overline{\gamma}^{q,i}_{b,m,j}}{\overline{\gamma}^{q,i}_{b,m,j} - \overline{\gamma}^{q,a}_{b,m,j}} \right) \left(1 - \sqrt{\frac{\overline{\gamma}^{q,i}_{b,m,j}}{1 + \overline{\gamma}^{q,i}_{b,m,j}}} \right) \right] \end{aligned} \tag{5.47}$$

According to the *Central Limit Theorem* (CLT), MUI can be incorporated into *Eq.* (5.47) by means of a GA [49, 50], or improved GA, at high user loads. This entails modelling the MUI as a zero mean Gaussian process with a variance of σ^2_{MUI}, and then adding this variance to the AWGN (see *Section* 2.2) variance present in *Eq.* (5.47) [50]. The variance σ^2_{MUI} will be a function of the type and the length of the spreading sequences used in the CDMA system, the received signal power of each CDMA user's signal at user-q's receiver, and most importantly, the number of users present in the CDMA system [50]. Although better approaches than the GA and improved GA are available to described MUI in DS/SSMA systems [113], these usually requiring more complex, higher order statistical analyses of the spreading sequences employed.

The complexity and scope this study's multi-user multipath fading performance evaluation platform, discussed in *Section* 5.4.3, far exceeds the mobile environment assumed during the derivation of the

theoretical BER performance curve of *Eq.* (5.47). Furthermore, *Eq.* (5.47)'s theoretical curve has several deficiencies, as discussed above. As such, this theoretical curve was not used for reference purposes during the examination of the simulated multi-user multipath fading channel BER performance results, presented in *Section* 6.5. Instead, Monte Carlo simulation results, presented by *Povey et al.* in [158] for a 32-tap RAKE receiver-based DS/SSMA system, are used for baseline reference purposes.

5.4 GENERAL SIMULATION CONFIGURATIONS

The following three subsections detail the general experimental setups for the AWGN, flat fading and multipath fading channel simulations of *Chapter* 6. This includes the transmitter, receiver and channel configurations employed in the simulation study.

5.4.1 SIMULATIONS IN AWGN CHANNEL CONDITIONS

Shown in *Fig.* 5.5 is the general narrowband complex QPSK communication system employed in the AWGN channel simulations of *Chapter* 6. For a specific E_b/N_0 ratio, this simulation platform

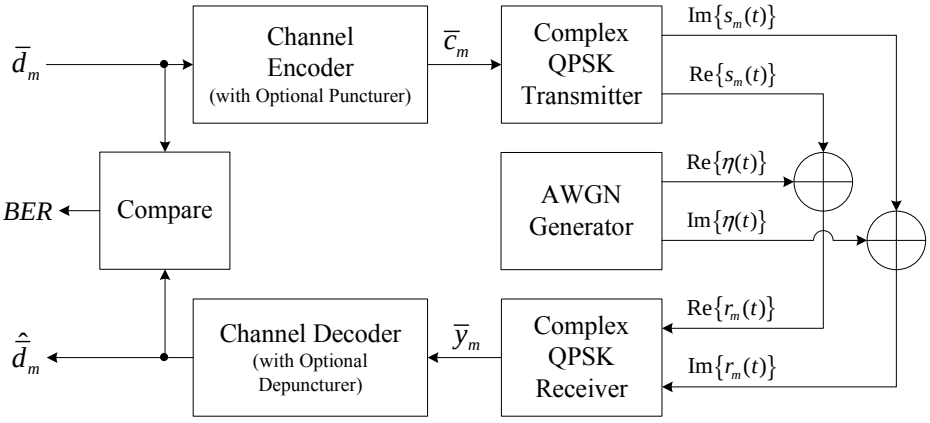

Figure 5.5: General AWGN Channel Simulation Platform

operates as follows: Firstly, the m^{th} data vector $\overline{d}_m$ is encoded by the channel encoder under investigation. If so required, the resultant set of code bits are then punctured (see *Section* 3.2.4), giving $\overline{c}_m$. Next, the transmitter creates the m^{th} set of complex QPSK symbols $\overline{s}_m(t)$ by modulating the code bits in $\overline{c}_m$. *Table* 5.1 details the general configuration of the transmitter structure. Most of these

Table 5.1: Narrowband Complex QPSK Transmitter Configuration

Configuration Option/Parameter	**Setting**
Symbol Rate [symbols/s]	1000
Effective RF Carrier [MHz]	900
Simulation RF Carrier [MHz]	0
Transmit Filters	None
Pulse Shaping Filters	Shaping: Square-Root Nyquist Roll-off Factor: $\varsigma = 0.5$
Modulation Approach	Balanced

parameters were arbitrarily chosen. For example, the QPSK symbol rate was conveniently chosen as 1000 symbols/s, since it has no bearing on the BER performance of such a system at a specific E_b/N_0 value in AWGN channel conditions. Although the simulations were performed completely in baseband, i.e. at a carrier frequency of 0 MHz, an effective RF frequency of 900 MHz was assumed, since this a common RF carrier frequency used in commercial wireless communication systems, such as GSM. The effective RF carrier has no real influence on the BER performance results obtained under AWGN channel conditions, but plays an important role in flat fading and frequency selective fading simulations.

As indicated by *Table* 5.2, square-root Nyquist pulse shaping [44, 154, 159, 160] was employed. A square-root Nyquist pulse is defined as follows:

$$h_{sqrt-Nyq}(t) = \left(\frac{1}{1-\left(\frac{4\varsigma t}{T_p}\right)^2}\right)\left[\left(\frac{1-\varsigma}{\sqrt{T_p}}\right)\left(\frac{\sin\left(\frac{\pi(1-\varsigma)t}{T_p}\right)}{\left(\frac{\pi(1-\varsigma)t}{T_p}\right)}\right)+\frac{4\varsigma}{\pi\sqrt{T_p}}\left(\cos\left(\frac{\pi\left(1+\varsigma\right)t}{T_p}\right)\right)\right] \tag{5.48}$$

where ς is the roll-off factor [44, 159, 160] of the pulse. In this study a roll-off factor of $\varsigma = 0.5$ was used. The parameter T_p represents the pre-pulse shaping symbol duration, which was set to $T_p = T_s$ for the narrowband simulations in AWGN and flat fading channel conditions. *Fig.* 5.6 depicts a normalised square-root Nyquist pulse for $\varsigma = 0.5$ and arbitrary T_p. Thus, for the transmitter of *Fig.* 5.1, $h_p^I(t) = h_p^Q(t) = h_{sqrt-Nyq}(t)$ with $T_p = T_s$. An estimate of the baseband transmitted signal's bandwidth is easily calculated as follows [47]:

$$B_{sig} = \frac{1}{2.T_s}(1+\varsigma) = 750 \text{ Hz} \tag{5.49}$$

Next, the QPSK modulated symbols experience the adverse effects of AWGN, presenting the nar-

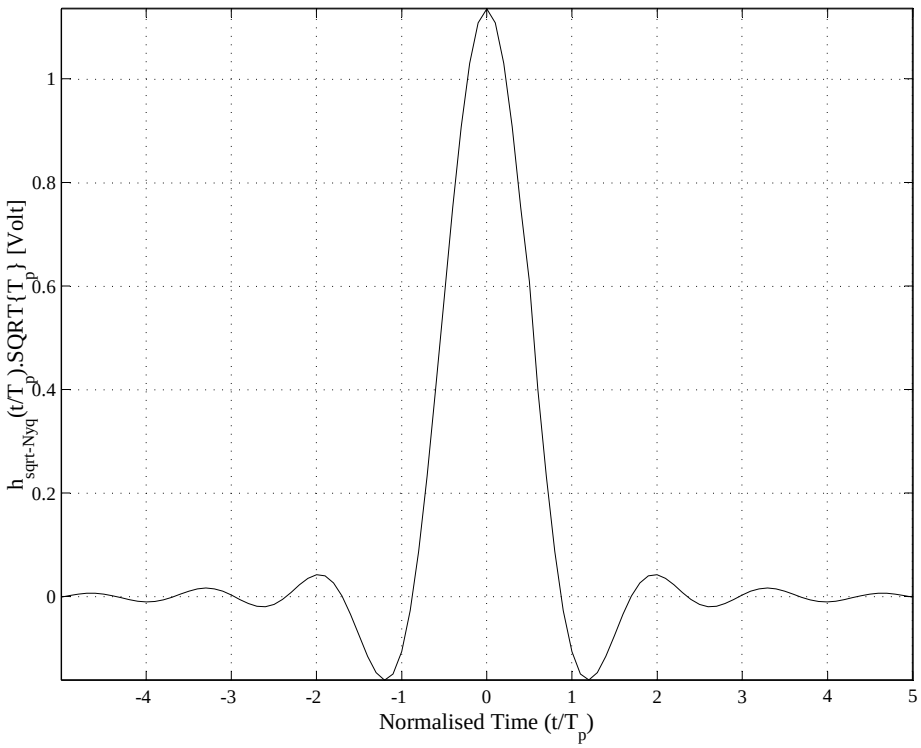

Figure 5.6: Normalised Square-Root Nyquist Pulse Shape for $\varsigma = 0.5$

rowband complex QPSK receiver, configured according to *Table* 5.2, with the m^{th} noisy input $\overline{r}_m(t)$. *Table* 5.2 states that the baseband receiver employs 6^{th} order lowpass elliptic receive filters [44, 114, 161] on the I-channel and Q-channel branches, which minimise the AWGN entering the receiver. Shown in *Fig.* 5.7 are the amplitude and phase responses of these filters, normalised with respect to the cutoff frequency f_{cut}. This type of lowpass filter was used, since it exhibits linear phase characteristics (see the bottom figure shown in *Fig.* 5.7). Note that $f_{cut} = 1000$ Hz, which was chosen somewhat larger than B_{sig} to ensure minimal phase distortion throughout the frequency band $0 \leq f \leq B_{sig}$. Furthermore, *Table* 5.2 states that square-root Nyquist matched filters are employed on the I-channel and Q-channel of the narrowband complex QPSK receiver. Thus, it follows that $h_m^I(t) = h_m^Q(t) = h_{sqrt-Nyq}(t)$ with $T_p = T_s$.

Table 5.2: Narrowband Complex QPSK Receiver Configuration

Configuration Option/Parameter	**Setting**
Symbol Rate [symbols/s]	1000
Effective RF Carrier [MHz]	900
Simulation RF Carrier	Baseband Simulation
Symbol Synchronisation	Perfect
Carrier Synchronisation	Perfect
Receive Filters	Type: Elliptic Order: 6 Cutoff Frequency [Hz]: $f_{cut} = 1/T_s = 1000$ Passband Ripple [dB]: 0.1 Stopband Attenuation [dB]: 40
Demodulation Approach	Balanced Matched Filtering
Matched Filters	Shaping: Square-Root Nyquist Roll-off Factor: $\varsigma = 0.5$

After demodulation, the channel decoder is presented with $\overline{y}_m$, a noisy estimate of the original code bits modulated by the narrowband complex QPSK transmitter. Before it attempts to decode $\overline{y}_m$, the channel decoder first restores possible punctured code bits by declaring the necessary erasures (see *Section* 3.3.4). Thereafter its decoding efforts produce $\hat{\overline{d}}_m$, which is an estimate of the original data bit vector $\overline{d}_m$. By comparing $\hat{\overline{d}}_m$ and $\overline{d}_m$, the number of errors incurred by the coded narrowband complex QPSK system for the m^{th} vector of data bits at the current E_b/N_0 is determined. Repeating the above process numerous times a statistically acceptable BER can be determined.

5.4.2 SIMULATIONS IN FLAT FADING CHANNEL CONDITIONS

Fig. 5.8 depicts the general simulation platform employed in the flat fading simulations of *Chapter* 6. Except for the addition of a complex flat fading channel simulator, this simulation platform is essentially identical to the AWGN channel simulation platform detailed in *Section* 5.4.1. As such, the narrowband complex QPSK transmitter and receiver, shown in *Fig.* 5.8, are also configured according to *Table* 5.1 and *Table* 5.2, respectively.

Table 5.3 details the complex flat fading channel configurations considered in *Chapter* 6. Recall

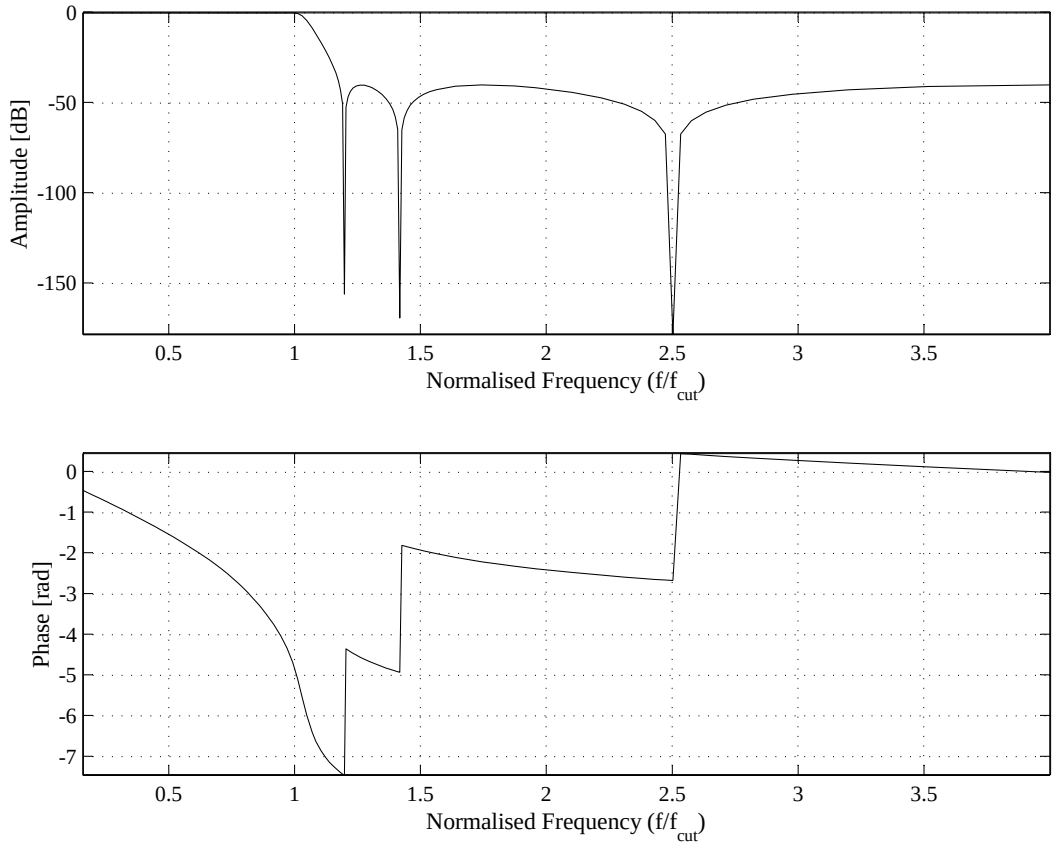

Figure 5.7: Amplitude and Phase Responses of the 6^{th} Order Lowpass Elliptic Receive Filters

Table 5.3: Possible Flat Fading Channel Simulator Configurations

Configuration Option/Parameter	**Settings Supported**
Rician Factors [dB]	$9, 6, 0, -100$
Doppler Spread [Hz]	100 (Velocity of 120 km/h, RF Carrier @ 900 MHz)
	67 (Velocity of 80 km/h, RF Carrier @ 900 MHz)
	33 (Velocity of 40 km/h, RF Carrier @ 900 MHz)

from *Table* 5.1 and *Table* 5.2 that an effective RF carrier frequency of 900 MHz is used. Thus, using *Eq.* (2.2) with an angle of arrival of $\theta_A(t) = 0$ rad, the supported Doppler spread frequencies of 33 Hz, 67 Hz and 100 Hz relate to relative transmitter-to-receiver velocities of 40 km/h, 80 km/h and 120 km/h, respectively. Recall from *Section* 5.4.1 that the QPSK transmitter's output signal has a bandwidth of approximately $B_{sig} = 750$ Hz. Since $B_D < B_{sig}$, it follows that the system experiences relatively slow flat fading. However, the ratio of signal bandwidth to Doppler spread is not large enough to assume a fading amplitude that remains essentially constant during one QPSK symbol period.

This simulation platform operates in a similar fashion as the AWGN channel simulation platform discussed in *Section* 5.4.1, with the exception of the following:

- Prior to the modulation of the channel coded bits by the narrowband complex QPSK transmitter, optional interleaving (see *Section* 3.2.3) is now also supported. At the receiver de-interleaving (see

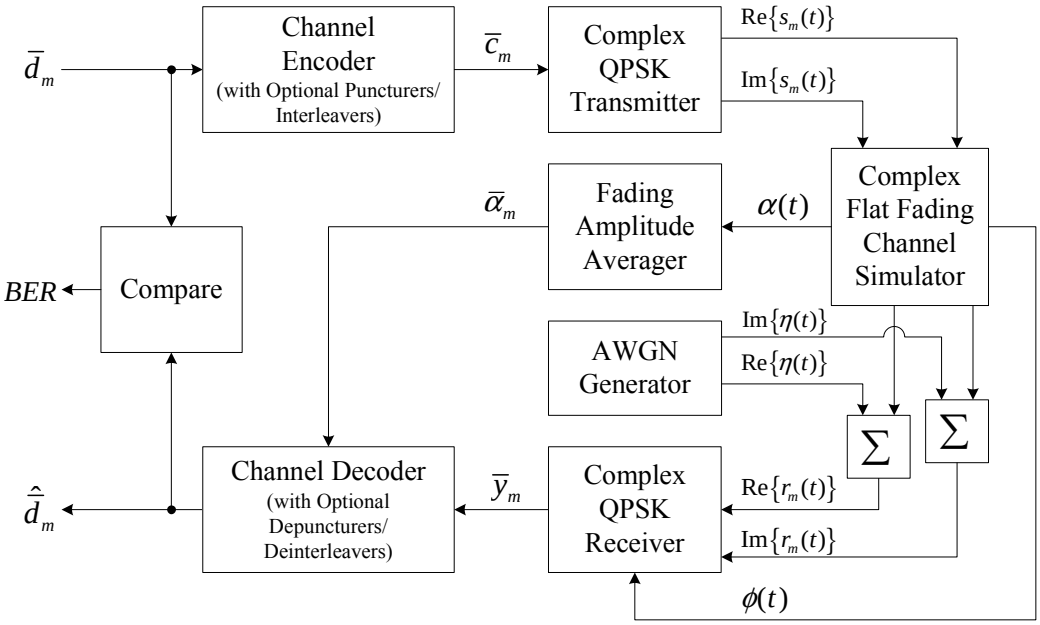

Figure 5.8: General Flat Fading Channel Simulation Platform

Section 3.3.3) can be performed to undo any interleaving introduced at the transmitter.

- The complex QPSK channel symbols experience not only the adverse effects of AWGN, but also that of flat fading, created by the complex flat fading channel simulator.
- The channel decoder is capable of using CSI, obtained directly from the complex flat fading channel simulator (see *Section* 2.6.2.5), in its decoding efforts.

5.4.3 SIMULATIONS IN FREQUENCY SELECTIVE FADING CHANNEL CONDITIONS

Fig. 5.9 depicts the frequency selective fading channel simulation platform used in this study [156]. This platform is built around the RAKE receiver-based complex DS/SSMA QPSK communication system discussed in *Section* 5.3. *Table* 5.4 summarises the general wideband transmitter configuration supported by each of the users in the CDMA environment. As stated in this table, this dissertation investigated the BER performances of coded wideband systems employing either unfiltered (see *Section* D.3.1), or filtered (see *Section* D.3.2) CSS families: With unfiltered CSS families, such as the *Zadoff-Chu* (ZC) and *Quadriphase* (QPH) families considered in this study, there is no bandlimiting built into the CSSs. Thus, additional pulse shaping is required to ensure effective spectrum utilisation. Similar to the narrowband simulation platforms discussed in the previous sections, square-root Nyquist pulse shaping is employed. However, pulse shaping is performed at CSS chip-level, i.e. the pulse shape $h_{sqrt-Nyq}(t)$ shown in *Fig.* 5.6 is employed with $T_p = T_{chip}$. Thus, for the pulse shaped CSS scenarios, the bandwidth of the baseband transmitter output signal can be approximated as follows:

$$B_{sig} = \frac{1}{2.T_{chip}}(1+\varsigma) = 47250 \text{ Hz} \tag{5.50}$$

In the case of the pre-filtered ABC and DSB CE-LI-RU filtered *Generalised Chirp-like* (GCL) CSSs, no additional bandlimiting is required, i.e. simple rectangular pulse shaping can be used. It has been shown that, when the spreading sequence length M_{seq} is sufficiently large, the *linearly interpolating root-of-unity* filtering technique [7, 8] employed in the generation of a DSB CE-LI-RU filtered GCL CSSs produces a signal bandwidth equivalent to that generated by Nyquist filtering with a roll-off

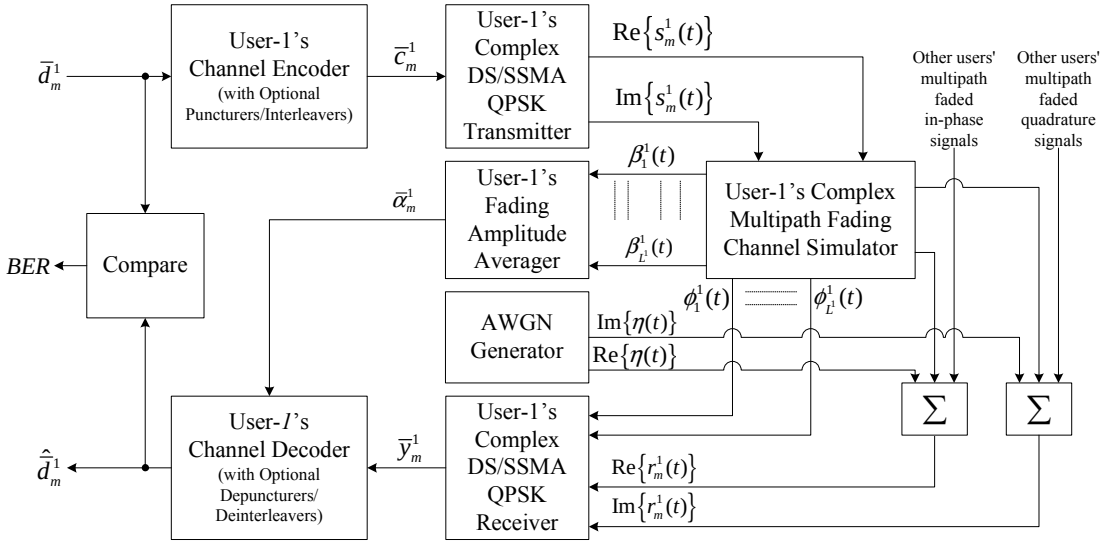

Figure 5.9: General Multipath Fading Channel Simulation Platform

factor approaching $\varsigma = 0$. Thus, the signal bandwidth of a baseband complex DS/SSMA QPSK communication system, configured to employ DSB CE-LI-RU filtered GCL CSSs, can be calculated as follows:

$$B_{sig} = \frac{1}{2.T_{chip}} = 31500 \text{ Hz} \tag{5.51}$$

In the case of the ABC sequences, balanced quadrature modulation will result in only the lower or upper sideband being transmitted, subsequently halving the required signal bandwidth:

$$B_{sig} = \frac{1}{4.T_{chip}} = 15750 \text{ Hz} \tag{5.52}$$

Up to 10 distinct CDMA users are supported by the simulation platform depicted in *Fig.* 5.9. However, only a single baseband complex RAKE receiver (user-1's receiver was used in this study) is present in the simulation platform, since only a single user's corrupted signal is demodulated and processed to determine the coded CDMA system's BER performance. Other users' signals present at this receiver's input create the MUI in the CDMA system. The BER performance of the RAKE receiver-based complex DS/SSMA QPSK communication systems in the presence of MUI is not only a function of the length of the CSSs employed (denoted by M_{seq}), but also the selection of good CSSs from a complete CSS family. This was found to be true for all of the CSS families considered, but especially for ABC sequences. In *Section* 6.5.1.3.2 and *Section* 6.5.1.3.3 in-depth studies are undertaken into the influence of these two factors on the BER performance of uncoded DS/SSMA QPSK communication systems employing ABC sequences.

For each of the 10 possible users in the CDMA system a unique complex multipath fading channel simulator (see *Section* 2.6.3.2) configuration was chosen, since the movement of the users' wideband complex transmitters relative to the single complex RAKE receiver is stochastic. However, perfect power control is assumed, i.e. the average powers of all the users' corrupted signals entering user-1's RAKE receiver are equal. Listed in *Table* 5.5 and *Table* 5.6 are the complex multipath fading channel simulator configurations for the 10 possible users. Each user's multipath fading channel simulator was configured to have 3 statistically independent paths, a choice frequently encountered in literature related to simulation studies on wideband CDMA systems. The Rician factor and Doppler spread for

Table 5.4: Wideband Complex DS/SSMA QPSK Transmitter Configuration

Configuration Option/Parameter	**Setting**
CSS Families Supported	ABC, DSB CE-LI-RU Filtered GCL, Unfiltered ZC, Unfiltered QPH
Unspreaded Symbol Rates [symbols/s]	1032.786 (Length-61 ABC Sequences) 984.375 (Length-64 ABC Sequences) 496.063 (Length-127 ABC Sequences) 1000 (All Length-63 Sequences)
Spreading Sequence Lengths [chips]	61 (Only ABC Sequences) 63 (All CSS Families) 64 (Only ABC Sequences) 127 (Only ABC Sequences)
Spreading Sequence Rate [chips/s]	63000
Effective RF Carrier [MHz]	900
Simulation RF Carrier [MHz]	0
Transmit Filters	None
Pulse Shaping Filters: Unfiltered Complex Spreading Sequences	Shaping: Square-Root Nyquist Roll-off Factor: $\varsigma = 0.5$
Pulse Shaping Filters: Filtered Complex Spreading Sequences	Shaping: Rectangular Roll-off Factor: N/A
Modulation Approach	Balanced
Power Control	Perfect

the i^{th} path of each user's channel simulator, respectively denoted by K_i and $B_{D,i}$, were randomly chosen from the options supported by the complex flat fading channel simulator, given in *Table* 5.3. Recalling the possible transmitter signal bandwidths for the different classes of CSSs, given by *Eq.* (5.50), *Eq.* (5.51) and *Eq.* (5.52), the different signal duration possibilities can be estimated as $T_{sig} = 1/B_{sig}$. With these signal bandwidths and durations known, each user's path powers and relative path delays, respectively denoted by τ_i and P_i, with $i = 1, 2, 3$, were chosen according to exponential decay power delay profiles (see *Section* 2.6.3.3) that conform to the requirements for frequency selective fading, i.e. $B_{sig} > B_C$ and $T_{sig} < \sigma_\tau$ (see *Section* 2.5.1.1). Note that the maximum excess delay (see *Section* 2.4.3.1) of user-1 is $\tau_{max} = 200$ μs, which is 12.6 CSS chips, or one fifth of a length-63 CSS in duration.

Table 5.7 details the complex DS/SSMA QPSK RAKE receiver's general configuration. Note that the lowpass elliptic receive filters employed in the RAKE receiver were identical to those used in the narrowband receivers, with the exception of the cutoff frequency, $f_{cut} = 1/T_{chip} = 63000$ Hz. Thus, *Fig.* 5.7, with $f_{cut} = 1/T_{chip}$, also depicts the frequency response of the wideband system's receive filters. Furthermore, the single RAKE receiver present in the CDMA system was configured to be perfectly synchronised with the received signal initially generated by user-1's wideband complex transmitter, i.e. perfect carrier, chip and symbol synchronisation were assumed on each of the RAKE taps.

Table 5.5: Complex Multipath Fading Channel Simulator Configurations for Users 1 to 5

		User Number				
		1	2	3	4	5
Path 1 **Setup**	P_1 [dB]	-0.1394	-0.3866	-0.2820	-0.5303	-1.0279
	$K_1[dB]$	9	9	9	9	9
	$B_{D,1}$ [Hz]	100	33	67	33	100
	τ_1 [μs]	0	20	30	10	40
Path 2 **Setup**	P_2 [dB]	-15.1394	-10.8866	-12.2820	-9.5303	-7.0279
	K_2 [dB]	0	0	0	0	0
	$B_{D,2}$ [Hz]	67	100	33	67	33
	τ_2 [μs]	100	90	110	70	80
Path 3 **Setup**	P_3 [dB]	-30.1394	-24.3866	-24.2820	-24.5303	-19.0279
	K_3 [dB]	-100	-100	-100	-100	-100
	$B_{D,3}$ [Hz]	33	67	100	100	67
	τ_3 [μs]	200	180	190	170	160
RMS Delay Spread σ_τ [μs]		18.286	21.288	21.108	20.947	20.208
Coherence Bandwidth B_C [Hz]		10937	9395	9475	9548	9897

Table 5.6: Complex Multipath Fading Channel Simulator Configurations for Users 6 to 10

		User Number				
		6	7	8	9	10
Path 1 **Setup**	P_1 [dB]	-0.3820	-0.2131	-0.3764	-0.2063	-0.5303
	$K_1[dB]$	9	9	9	9	9
	$B_{D,1}$ [Hz]	67	100	67	33	33
	τ_1 [μs]	20	30	10	0	30
Path 2 **Setup**	P_2 [dB]	-10.8820	-13.7131	-10.8764	-13.7063	-9.5303
	K_2 [dB]	0	0	0	0	0
	$B_{D,2}$ [Hz]	100	100	67	33	67
	τ_2 [μs]	90	120	80	90	90
Path 3 **Setup**	P_3 [dB]	-25.8820	-22.7131	-28.8764	-24.2063	-24.5303
	K_3 [dB]	-100	-100	-100	-100	-100
	$B_{D,3}$ [Hz]	33	67	33	67	33
	τ_3 [μs]	190	180	200	160	190
RMS Delay Spread σ_τ [μs]		20.897	21.060	20.288	20.555	20.947
Coherence Bandwidth B_C [Hz]		9571	9497	9858	9730	9548

Table 5.7: Wideband Complex DS/SSMA QPSK RAKE Receiver Configuration

Configuration Option/Parameter	**Setting**
CSS Families Supported	ABC, DSB CE-LI-RU Filtered GCL, Unfiltered ZC, Unfiltered QPH
Unspreaded Symbol Rates [symbols/s]	1032.786 (Length-61 ABC Sequences) 984.375 (Length-64 ABC Sequences) 496.063 (Length-127 ABC Sequences) 1000 (All Length-63 Sequences)
Spreading Sequence Lengths [chips]	61 (Only ABC Sequences) 63 (All CSS Families) 64 (Only ABC Sequences) 127 (Only ABC Sequences)
Spreading Sequence Rate [chips/s]	63000
Effective RF Carrier [MHz]	900
Simulation RF Carrier [MHz]	0
Receive Filters	Type: Elliptic Order: 6 Cutoff Frequency [Hz]: $f_{cut} = 63000$ Passband Ripple [dB]: 0.1 Stopband Attenuation [dB]: 40
Matched Filters: Unfiltered Complex Spreading Sequences	Shaping: Square-Root Nyquist Roll-off Factor: $\varsigma = 0.5$
Matched Filters: Filtered Complex Spreading Sequences	Shaping: Rectangular Roll-off Factor: N/A
Demodulation Approach	Balanced Matched Filtering
RAKE Receiver Configuration	MRC, Perfect Knowledge of Path Delays and Instantaneous Fading Amplitudes
Symbol Synchronisation	Perfect for Each RAKE Receiver Tap
Carrier Synchronisation	Perfect for Each RAKE Receiver Tap
Code Lock	Perfect for Each RAKE Receiver Tap

The frequency selective fading channel simulation platform shown in *Fig.* 5.9 operates as follows: Firstly, user-1's m^{th} data bit vector $\overline{d}_m^1$ is encoded by the channel coder under investigation. If so required, the channel coded bits are interleaved and/or punctured to give $\overline{c}_m^1$. The vector $\overline{c}_m^1$ is modulated by user-1's baseband complex DS/SSMA QPSK transmitter to give $\overline{s}_m^1(t)$. The output $\overline{s}_m^1(t)$ is now processed by user-1's complex multipath fading channel simulator. Similar processing is done by the other users' multipath fading channel simulators on their respective modulated symbols. Next, the channel simulator outputs are summed, followed by the addition of AWGN. The result is user-1's complex RAKE receiver input $\overline{r}_m^1(t)$. This input is demodulated by the complex RAKE receiver, giving $\overline{y}_m^1$, which is a soft estimate of $\overline{c}_m^1$. Following possible de-puncturing and/or de-interleaving of $\overline{y}_m^1$, the channel decoder creates an estimate of $\overline{d}_m^1$, denoted by $\hat{\overline{d}}_m^1$. Repeating the process described above numerous times, comparing $\overline{d}_m^1$ and $\hat{\overline{d}}_m^1$ for each encoding instance, the BER performance of the coded RAKE receiver-based complex DS/SSMA QPSK communication system can be estimated for the current channel conditions.

5.5 CONCLUDING REMARKS

This chapter set out to describe the performance evaluation platforms implemented in the simulation study of this dissertation. Firstly, the operation, average fading amplitude calculation and theoretical BER performances of the narrowband complex QPSK communication system employed in the AWGN and flat fading channel simulations of *Chapter* 6 were considered. This was followed by a similar discussion on the wideband RAKE receiver-based complex DS/SSMA QPSK communication system, employed in *Chapter* 6's frequency selective fading channel simulations. Lastly, *Chapter* 6's AWGN, flat fading and frequency selective fading channel simulation platforms, constructed using the above mentioned narrowband and wideband communication systems, were described in detail. Listed below are the unique contributions that were made in this chapter:

1. *Section* 5.2 describes the operation and theoretical BER performances of a novel baseband complex QPSK communication system. This model is ideal for simulation purposes, since it negates the use of high sampling frequencies. A novel average fading amplitude CSI calculation technique is presented in *Section* 5.2.3.

2. A unique baseband RAKE receiver-based complex DS/SSMA QPSK communication system is presented in *Section* 5.3. The general operation of the baseband complex DS/SSMA QPSK transmitter and RAKE receiver structures are detailed in this subsection. *Section* 5.3.3 describes a simple, but innovative method whereby average fading amplitude CSI can be calculated for each of the output demodulated code bits after the RAKE receiver's MRC demodulation efforts. Lastly, a simplified theoretical derivation of the wideband system's multipath fading channel BER performance, in the absence of MUI, is considered.

3. A flexible baseband simulation platform, suitable for AWGN channel performance testing of channel coding schemes, is presented in *Section* 5.4.1. This platform employs the narrowband complex QPSK transmitter and receiver structures of *Section* 5.2. Furthermore, this platform includes realistic pulse shaping and receiver filters in order to ensure the authenticity of the simulation results presented in *Chapter* 6.

4. Also built around the baseband complex QPSK transmitter and receiver structures described in *Section* 5.2, is the baseband flat fading channel simulation platform described in *Section* 5.4.2. This platform employs the novel complex implementation of *Clarke*'s flat fading channel simulator model, presented in *Section* 2.6.2.3. A number of frequently encountered Doppler spread frequencies and Rician factors are supported by this simulation platform, making it possible to

determine the BER performances for channel coding schemes in a multitude of realistic flat fading channel conditions.

5. *Section* 5.4.3 presents one of the major contributions of this dissertation, namely a baseband multi-user multipath fading channel simulation platform, employing RAKE receiver-based complex DS/SSMA QPSK communication systems (see *Section* 5.4.3). Not only is this simulation platform a useful tool with which the communications engineer can determine the effects of multipath fading on different channel coding schemes, but it also supports multi-user CDMA experiments. Since each user's wideband transmitter output signal is processed by an individual complex multipath fading channel simulator, realistic wideband multi-user mobile communication environments can be recreated.